Comparative Protein Modeling of 1-Deoxy-D-xylulose-5-phosphate Reductoisomerase Enzyme from *Plasmodium falciparum*: A Potential Target for Antimalarial Drug Discovery

Nidhi Singh,[†] Gwénaël Chevé,[†] Mitchell A. Avery,[†,§,||] and Christopher R. McCurdy*[,†,‡]

Department of Medicinal Chemistry, Laboratory for Applied Drug Design and Synthesis, Department of Pharmacology, School of Pharmacy, National Center for Natural Products Research, and Department of Chemistry and Biochemistry, University of Mississippi, University, Mississippi 38677-1848

Received December 2, 2005

Plasmodium falciparum 1-deoxy-D-xylulose-5-phosphate reductoisomerase (*Pf*-DXR) is a potential target for antimalarial chemotherapy. The three-dimensional model (3D) of this enzyme was determined by means of comparative modeling through multiple alignment followed by intensive optimization, minimization, and validation. The resulting model demonstrates a reasonable topology as gauged from the Ramachandran plot and acceptable three-dimensional structure compatibility as assessed by the Profiles-3D score. The modeled monomeric subunit consists of three domains: (1) N-terminal NADPH binding domain, (2) connective or linker domain (with most of the active site residues located in this domain), and (3) a C-terminal domain. This structure proved to be consistent with known DXR crystal structures from other species. The predicted active site compared favorably with those of the templates and appears to have an active site with a highly conserved architecture. Additionally, the model explains several site-directed mutagenesis data. Besides using several protein structure-checking programs to validate the model, a set of known inhibitors of DXR were also docked into the active site of the modeled *Pf*-DXR. The docked scores correlated reasonably well with experimental pIC_{50} values with a regression coefficient (R^2) equal to 0.84. Results of the current study should prove useful in the early design and development of inhibitors by either de novo drug design or virtual screening of large small-molecule databases leading to development of new antimalarial agents.

INTRODUCTION

Malaria is a major public health problem in the world—with an estimated 300−500 million new clinical cases each year causing 1.1−2.7 million deaths annually, with most of the deaths among children.[1] Current empirical estimates suggest that the total could run as high as 660 million.[2] It is estimated that approximately 40% of the world population is at risk of infection with malaria.[3] Today, the threat is most significant for nations in Africa, Asia, Latin America, and some regions of the South Pacific. This disease is caused by protozoa of the genus *Plasmodium*.[4] Four different species of this blood-borne apicomplexan pathogen, *P. falciparum*, *P. vivax*, *P. ovale*, and *P. malariae*, cause malaria in humans,[5] which can be transmitted by about 60 species of *Anopheles* mosquito. Particularly, *P. falciparum* is the most severe and life-threatening form of malaria causing parasite.[6] Control of malaria has been severely compromised by the development of malarial parasites resistant to nearly all antimalarial drugs used for prophylaxis and treatment. The prospect for a marketable malaria vaccine within the near future is unlikely, and control of transmission vectors seems impractical. Consequently, the need for novel chemotherapeutic approaches in the fight against multiresistant *P. falciparum* is imperative.

The availability of the genome sequence of *P. falciparum*,[7] and especially the wealth of information on the biochemical pathways used by this organism, has opened novel approaches for drug development. One such pathway is the 1-deoxy-D-xylulose 5-phosphate/2-C-methyl-D-erythritol-4-phosphate (DXP/MEP) pathway[8] which has been shown to represent an effective target for chemotherapy of malaria. Discovery of this pathway in the apicoplast of malarial parasite, *P. falciparum*,[9] essential for the growth and survival of the pathogen has stimulated extensive research in this area. Interestingly, this pathway is also found operative in most eubacteria including several pathogenic species such as *Mycobacterium tuberculosis*, *Helicobacter pylori*, *Haemophilus influenzae*,[10] in algae,[11] and in the plastids of plant cells.[12] It is, however, absent in mammals, fungi, and the cytosol of plant cells which instead use the mevalonate pathway[13] for isoprenoid synthesis. Given the essential nature of the DXP/MEP pathway in these organisms and the absence of this pathway in humans, the constituent enzymes of the DXP/MEP pathway offer the potential for novel therapeutic intervention, perhaps without toxicity to vertebrates.

DXR is the first enzyme committed to isoprenoid biosynthesis in the MEP pathway (Figure 1). It is responsible for the conversion of DXP to MEP, in the presence of a cofactor, nicotinamide adenine dinucleotide phosphate (NADPH), and

* Corresponding author phone: (662)915-5882; fax: (662)915-5638; e-mail: cmccurdy@olemiss.edu.
[†] Department of Medicinal Chemistry, Laboratory for Applied Drug Design and Synthesis.
[‡] Department of Pharmacology, School of Pharmacy.
[§] National Center for Natural Products Research.
[||] Department of Chemistry and Biochemistry.

10.1021/ci050523w CCC: $33.50
Published on Web 04/04/2006

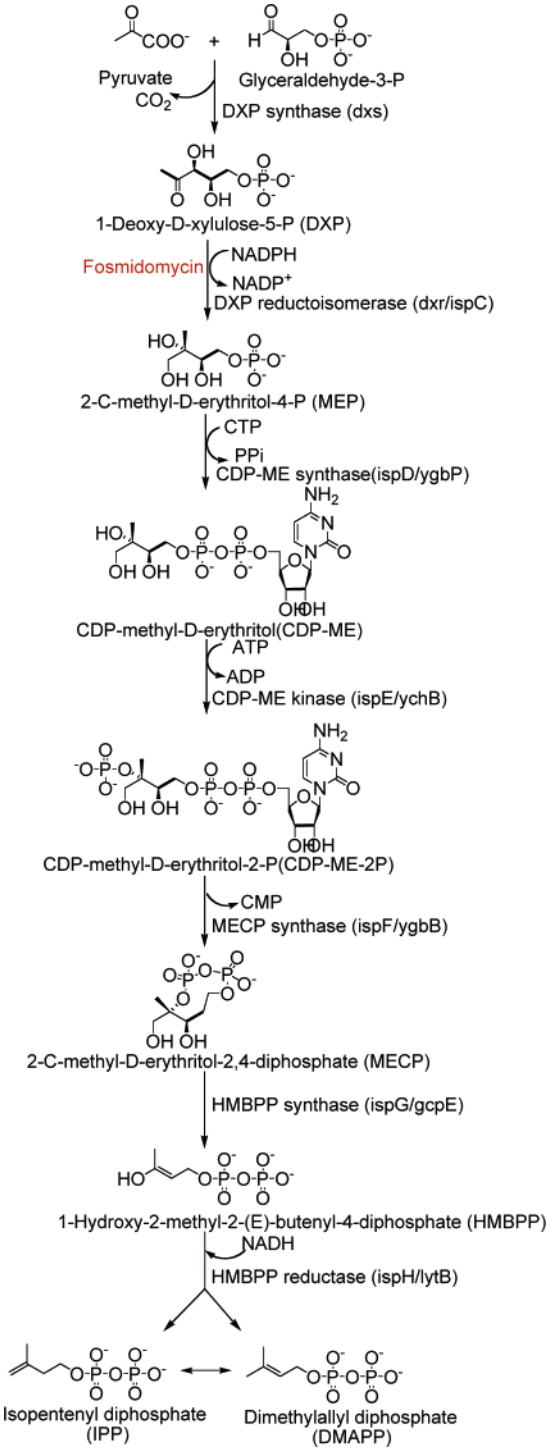

Figure 1. Outline of the DXP pathway for the biosynthesis of IPP. The enzymes responsible for catalyzing each step are indicated, while the corresponding genes are within parentheses. The inhibitor fosmidomycin that blocks the second step of the pathway is highlighted in red.

a divalent metal ion (Mg^{2+} or Mn^{2+}). DXP is a precursor not only for isopentenyl diphosphate, the common metabolic precursor of all isoprenoids, but also thiamine (vitamin B_1)[14] and pyridoxal (vitamin B_6).[15−17] Fosmidomycin (Figure 2), a natural antibiotic from *Streptomyces lavendulae*,[18] has been identified as a specific, mixed type (competitive and non-competitive) inhibitor of DXR (K_i of 38 nM against *Escherichia coli* and 300 nM against *Zymomonas mobilis* DXR enzyme).[9,19,20] Fosmidomycin possesses potent anti-

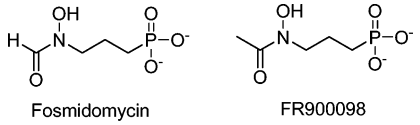

Figure 2. The chemical structures of known inhibitors of the DXR enzyme.

malarial activity in vitro and has also been shown to prevent murine malaria.[9] In a recent clinical study, fosmidomycin was shown to be effective and well tolerated in the treatment of patients with acute uncomplicated *Plasmodium falciparum* malaria.[21] These findings imply that DXR is a valid target, and inhibitors of this enzyme could serve as potential leads for malarial chemotherapy.

With the X-ray crystallographic structure of an enzyme known, the drug design process is significantly facilitated. However, one is frequently faced with the situation where a ligand must be designed for a target protein for which no experimentally determined structure is available. It is in such cases that comparative protein structure modeling can be employed to build a three-dimensional model for a protein of unknown structure on the basis of sequence similarity to related proteins of known 3D structure.[22] The comparative approach to protein structure prediction is based on the fact that structure is more conserved than the sequence during evolution. Therefore, similar sequences exhibit nearly identical structures,[23] and even proteins that share low or even nondetectable sequence similarity many times also have similar structures.[24]

Therefore, in the absence of a well-defined structure of *Pf*-DXR, comparative protein modeling provided a rational alternative to develop a reasonable three-dimensional (3D) model. Homology modeling is usually the method of choice when a clear relationship of homology between the sequence of the target protein and at least one known X-ray crystallographic structure is found. This approach produces a reasonable structural model for protein sequence with available related templates having more than 25% amino acid sequence identity.[25] Generally, it is assumed that the tertiary structures of the two proteins will be similar if their sequences are related.[26] In the present work, construction of a 3D model for the DXR using the X-ray crystal structures of the enzyme DXR from *E. coli* (PDB Id: 1Q0L) and *Z. mobilis* (PDB Id: 1R0L) as templates that share 36.2% and 36.5% sequence identity with the *P. falciparum* sequence, respectively, has been reported. For such a sequence identity, homology modeling yields a structure that is accurate enough for use in subsequent computational studies.[27] The resulting model was validated with various structure/geometry verification tools as well as automated docking simulation studies of known inhibitor molecules. The docking studies also provided insight into the possible binding modes and interactions of ligands with the modeled enzyme.

COMPUTATIONAL METHODS

All modeling was performed using commercial softwares from MSI/Biosym Technologies (San Diego, CA) and Tripos Inc. (St. Louis, MO). Computational studies were performed on a Silicon Graphics Octane 2 workstation, equipped with two parallel R12000 processors.

HOMOLOGY MODELING

Building protein models by homology normally proceeds along a series of reasonably well-defined steps: (1) sequence alignment between the target and the template; (2) building an initial model; (3) refining the model; and (4) evaluating the model.

Sequence Alignment. The peptide sequence of *P. falciparum* DXR comprised of 488 amino acid residues was retrieved from the SWISSPROT protein sequence data bank (http://us.expasy.org/sprot/; accession no. 096693).[28] The protein sequence of the DXR from *P. falciparum* consists of a unique NH_2-terminal extension, the first 30 amino acids of which resemble an endoplasmic reticulum signal peptide. The following 44 amino acids present in the NH_2-terminal exhibit the characteristics of plastidial targeting sequences.[9] For that reason, the *P. falciparum* DXR enzyme was modeled with these residues deleted. Sequence alignment was then derived with the CLUSTALW v.1.8 package[29] using the BLOSUM matrices for scoring the alignments. The parameter for GAP OPEN, GAP EXTENSION, and GAP DISTANCE were set equal to 10, 0.2, and 8, respectively. Obtaining a high quality multiple sequence alignment of the target with the templates is a crucial step in protein homology modeling, since only small local errors made in alignment can be corrected in the subsequent steps. Openings and extension GAP penalty were changed systematically, and the obtained alignment was then manually refined and inspected for structural integrity in the structurally conserved regions of the available crystal structure. The PHD algorithm[30] was used to predict the secondary structure of *Pf*-DXR.

Generation of Initial Model. Following the alignment, the backbone coordinates of the residues in *Pf*-DXR were generated with the *InsightII*/HOMOLOGY module version 2000.[31] Regions in the *Pf*-DXR enzyme that aligned with the structurally conserved regions (SCRs) among the two templates were generated by copying the backbone coordinates from one of the templates. *Ec*-DXR was generally used for this purpose, since it is the only template known in a ternary complex with NADPH and fosmidomycin and reveals a tight binding closed conformation.[32] To construct the backbone of non-SCR regions, two different procedures were used. If the sequence length was the same for both, the backbone coordinates from *Ec*-DXR were used for *Pf*-DXR. Otherwise, a loop search of the structures in the PDB data bank was performed. When loop searches were performed, trial loops were generated from the PDB by InsightII/HOMOLOGY. The criteria for loop selection were the correct number of residues in the loop, the distance between the ends, and the secondary structure adjacent to both ends. In each case, 10 loop structures were presented, and the final choice was made on the best fit, as assessed predominantly by the deviation and root-mean-squared deviation (RMSD) values. Deviation refers to how closely the loop matches the distance between the open ends. RMSD provides a measure of how well the conformation of the 'tails' (the five residues either side of the loop) of the selected loop match the 'tails' on the model being constructed. In both cases, the smaller the number the better, and it should be <2.0. The loop splice function is used to repair the omega angles and distances of where the loops are joined, to 180° and 1.34 Å, respectively. Following construction of the initial backbone model, initial side-chain conformers were generated.

After the initial model was completely built, the side chains were modeled further by using the SCWRL 3.0 software.[33,34] It has been found that the template and the target X-ray crystal structure have different rotamers for up to 45% of the conserved residues; therefore, side-chain conformations should be modeled on the basis of more general physical principles rather than by simply mimicking those of the template.[35] Many different strategies for assigning side-chain conformations in 3D models of proteins have been described in the literature. SCWRL 3.0 is one such program that was used to generate appropriate side-chain conformations for each residue in *Pf*-DXR. In this program, side-chain conformations are selected to add to a protein backbone based on a backbone-dependent rotamer library. In this library, lists of $\chi1-\chi2$ pairs for residues at given $\varphi-\psi$ values are provided. The best pairs are then explored to minimize side-chain-backbone and side-chain-side-chain steric repulsions. This resulted in a complete model of the protein, including all backbone and side-chain atoms.

Model Refinement. This initial model was energy-minimized, employing the *InsightII*/DISCOVER module, using 100 steps of steepest descents and 300 steps of conjugate gradients with a CVFF force field. During the initial minimizations, the backbone atoms of the SCRs of *Pf*-DXR were kept fixed. Loop atoms were not fixed since the final conformations of the loops are usually altered significantly from their original structures, as found by Homology modeling/Loop Search.

Protein−Ligand Complex Formation. For the purpose of complex protein formation, fosmidomycin, Mg^{2+} ion, and a tightly bound water molecule in the binding site were extracted from the *Ec*-DXR crystal structure (PDB Id: 1ONP). Bond orders and the correct protonation state were assigned upon visual inspection. The coordinates for the cofactor (NADPH) were transferred from PDB Id: 1Q0L, and the same procedure was applied as above. A subsequent minimization of the transferred cofactor with the CVFF force field, as implemented in biopolymer module of *InsightII*, revealed no significant movements. The metal ion, Mn^{2+} present in the crystal structure (PDB Id: 1ONP), was converted to Mg^{2+} since it is the relevant divalent cation in vivo[36−38] and also because the softwares used in this study are better suited for magnesium ion. Besides, it has been established that these ions are interchangeable owing to their closely related coordination properties.[39]

Finally, the main molecular mechanics minimization was performed using the DISCOVER module of *InsightII* and a CVFF force field. The procedure consisted of the following five steps: (1) the model was soaked with a 5 Å water layer, (2) water and model hydrogens were minimized in 600 steps, (3) side chains without active site side chains were minimized in 1000 steps, (4) active site side chains and the docked cofactor, fosmidomycin, a critical binding site water molecule, and metal ion (Mg^{2+}) were minimized in 1000 steps, and (5) the entire model with all ligands was minimized until the maximum derivative was less than 0.001 kcal/mol Å.

Model Evaluation. The model quality was assessed using a variety of validation tools. The PROSTAT module of *InsightII* was used to analyze the properties of bonds, angles, and torsions. The PROFILE-3D program in *InsightII* was

used to check the structure and sequence compatibility, while the PROCHECK suite of programs[40] was used for assessing the "stereochemical quality" of the modeled protein structure. Also, root-mean-square deviation (RMSD) values were calculated for the minimized homology model and compared to the template structures. RMSDs were also calculated for the structures before and after minimization to show there were no gross movements, which would indicate whether the templates used were suitable.

Automated Docking Simulations. Docking runs were performed using the GOLD v. 2.1 (Genetic Optimization for Ligand Docking)[41] program that uses a genetic algorithm (GA) to explore the full range of ligand conformational flexibility and the rotational flexibility of selected receptor hydrogens.[42] The mechanism for ligand placement is based on fitting points. The program adds fitting points to hydrogen-bonding groups on protein and ligand and maps acceptor points in the ligand on donor points in the protein and vice versa. Additionally, GOLD generates hydrophobic fitting points in the protein cavity onto which ligand CH groups are mapped. The GA optimizes flexible ligand dihedrals, ligand ring geometries, dihedrals of protein OH and NH_3^+groups, and the mappings of the fitting points. The docking poses are ranked based on a molecular mechanics-like scoring function, which includes a hydrogen bond term, a 4−8 intermolecular van der Waals terms, and a 6−12 intramolecular van der Waals term for the internal energy of the ligand.

The protein input was prepared by removing fosmidomycin from the final protein complex. Overall 20 inhibitors with known activities against DXR[43] that spanned an activity range of 4 log orders were built and minimized for 1000 steps each of steepest descents followed by conjugate gradients and finally by the BFGS method to a gradient of 0.001 kcal/mol/Å or less using the *InsightII*/Builder module. All atom types and charges were assigned in GOLD. Standard default settings were used for all calculations, with the exception that 15 GA runs were performed instead of 10. GOLD terminates when the top three dockings are within 1.5 Å of each other. The binding pocket was defined as a spherical region of 12 Å radius centered from the side-chain nitrogen atom of Asn237. This sphere encompasses all residues known to be involved in inhibitor binding.[32] The selection of the most appropriate docking solutions was based on a suitable placement of the phosphonate moiety and an octahedral coordination geometry around the metal ion.

RESULTS AND DISCUSSION

To date, several crystal structures of DXR from *E. coli*[32,44−47] and one from *Z. mobilis*[48] have been reported by different research groups. The first published crystal structure of *E. coli* DXR was an apoenzyme, which revealed the arrangement of the three domains—an amino terminal dinucleotide binding domain, a connective domain, and a carboxy terminal four-helix bundle domain, to form an overall V-shaped molecule with an apparent flexibility observed in the loop region.[44] The second structure also was of the *E. coli* DXR complexed with NADPH and a sulfate ion. This structure provided insight into the cofactor binding that stabilized the protein molecule and exhibited a more ordered flexible loop region. The sulfate ion was found positioned within the putative phosphate binding pocket in the DXR protein.[45] The first DXR-ligand complex structure with Mn^{2+} and fosmidomycin bound was reported along with two other structures of DXR: the apoenzyme and with Mn^{2+}. Unfortunately, the NADPH binding site was blocked by the C-terminus of neighboring monomer in the crystal. Consequently, the catalytic loop region was also found to be only partially ordered, and no structural rearrangement within the enzyme was observed assuming that complete ordering of the loop region requires substrate as well as cofactor binding within the binding pocket.[46] The structure of *Z. mobilis* DXR in the apo-form and as a binary complex with NADPH was solved. Comparison with the *E. coli* DXR crystal structures revealed that except for differences in the residues interacting with the adenine ring of NADPH, the two enzymes shared significant structural homology and highly conserved active site architecture.[48] Crystallographic structures of two biphosphonate inhibitors complexed to DXR were published, but neither NADPH nor a metal ion is present in either structure. Instead, a sulfate ion is observed which fits to the substrate phosphate pocket in a similar fashion as seen in one of the previous crystal structures.[45] However, the binding mode of these inhibitors is completely different when compared to the DXR-fosmidomycin complex.[47] Recently, the ternary structures of the DXR-NADPH-fosmidomycin, the DXR-NADPH-substrate, and the selenomethionine-labeled DXR-NADPH-fosmidomycin complex in a tight binding closed enzyme conformation were solved. The DXR-NADPH-fosmidomycin complex revealed a binding mode of fosmidomycin not mediated by a metal ion, although a model of metal-mediated inhibitor binding was proposed in the paper. The absence of expected metal ion from the structure was attributed to the acidic crystallization conditions (pH = 5) used at which the affinity of DXR for metal is low. Furthermore, this structure had a fully ordered loop conformation that closed upon the active site making interactions with the ligand.[32] The 3D structure of *Pf*-DXR is not yet known, but the enzyme is a logical target for structure based molecular design. Therefore, a homology model was developed using 3D coordinates of *Ec*-DXR in a tight binding closed conformation which should logically be closer to the conformation adopted by the enzyme in a physiological environment and therefore serves as better tool to understand the critical ligand-protein interactions.

Sequence Alignment. The final alignment of the deduced amino acid sequence of the *Pf*-DXR from the homologous enzymes from *E. coli* (PDB Id: 1Q0L) and *Zymomonas mobilis* (PDB Id: 1R0L) used for model building is shown in Figure 3. A total of 8 structurally conserved regions (SCRs) were conceived which constituted the major segment (about 95.35%) of total sequence. The remaining parts of the sequence, the structurally variable regions (SVRs), were not in close proximity of the binding pocket. Using this alignment, the 3D structure of *Pf*-DXR was generated using the HOMOLOGY MODELING module in the *InsightII* program. The resulting structure consisted of three domains: a larger N-terminal NADPH binding domain comprising 157 residues, a connective or linker domain (residues 167−280), and a smaller C-terminal alpha-helical domain comprising residues 313 to 414. The N-terminal domain, a variant of the classical nucleotide-binding domain, exhibited an α/β topology with a seven-stranded parallel β-sheet and

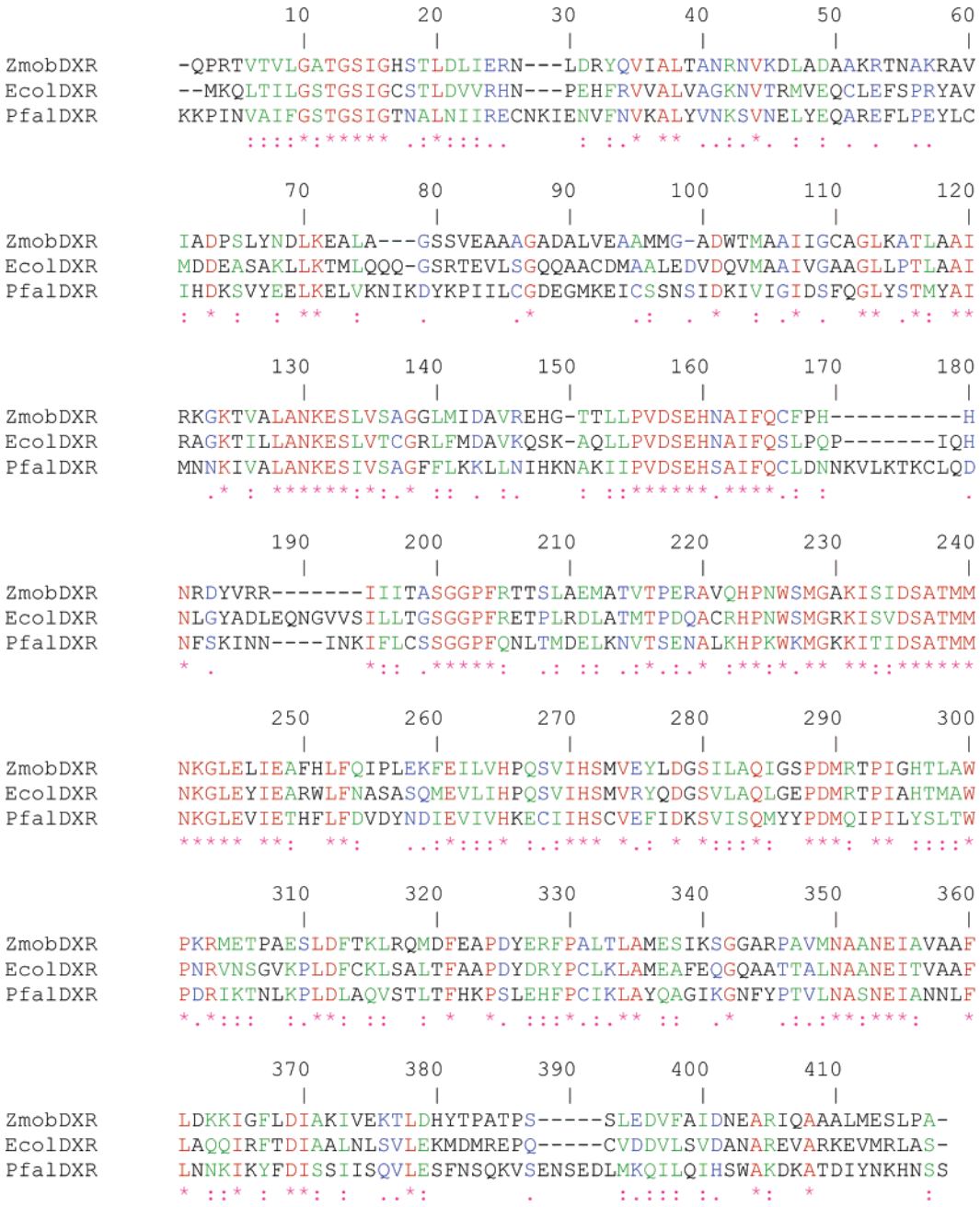

Figure 3. Multiple sequence alignment using ClustalW. Alignment length: 418 residues; identity (red *): 110 is 26.32%; strongly similar (green :): 94 is 22.49%; weakly similar (blue .): 50 is 11.96%; different: 164 is 39.23%.

seven α-helices. The connective domain comprises five helices and a four-stranded β-sheet with one parallel and two antiparallel alignments. The smaller C-terminal domain consisted of a four-helix bundle and is joined to the connective domain by an extended loop (residues 216−226), which spans the entire central domain.

Energy Minimization and Model Refinement. The quality of the initial model was improved by subjecting it to a crude energy minimization protocol. These minimizations produced a model with correct bond lengths and bond angles and where individual atoms are not too close together.

Binding of an inhibitor to the active site of an enzyme is typically associated with local and, perhaps, also global structural rearrangement of the enzyme (induced-fit mechanism). As a result, structure-based drug design preferentially relies on the structures of enzyme−inhibitor complexes containing bound inhibitors. Keeping this in mind, the next step was developing a protein−ligand complex that would offer a more detailed and accurate picture of the inhibitor−enzyme interactions and structural complementarity between the inhibitor and the active site. Such a protein−ligand complex may be used more appropriately to perform docking simulation studies and may provide more meaningful docking solutions.

Therefore, a protein−ligand complex was developed from the initially generated homology model of the target protein by including information about known ligands as spatial restraints and optimizing the mutual interactions between the ligands and the binding sites. Assuming that the ligand binding modes are similar in the target and the template protein structures, the coordinates of ligands were transferred from the known DXR crystal structures keeping their

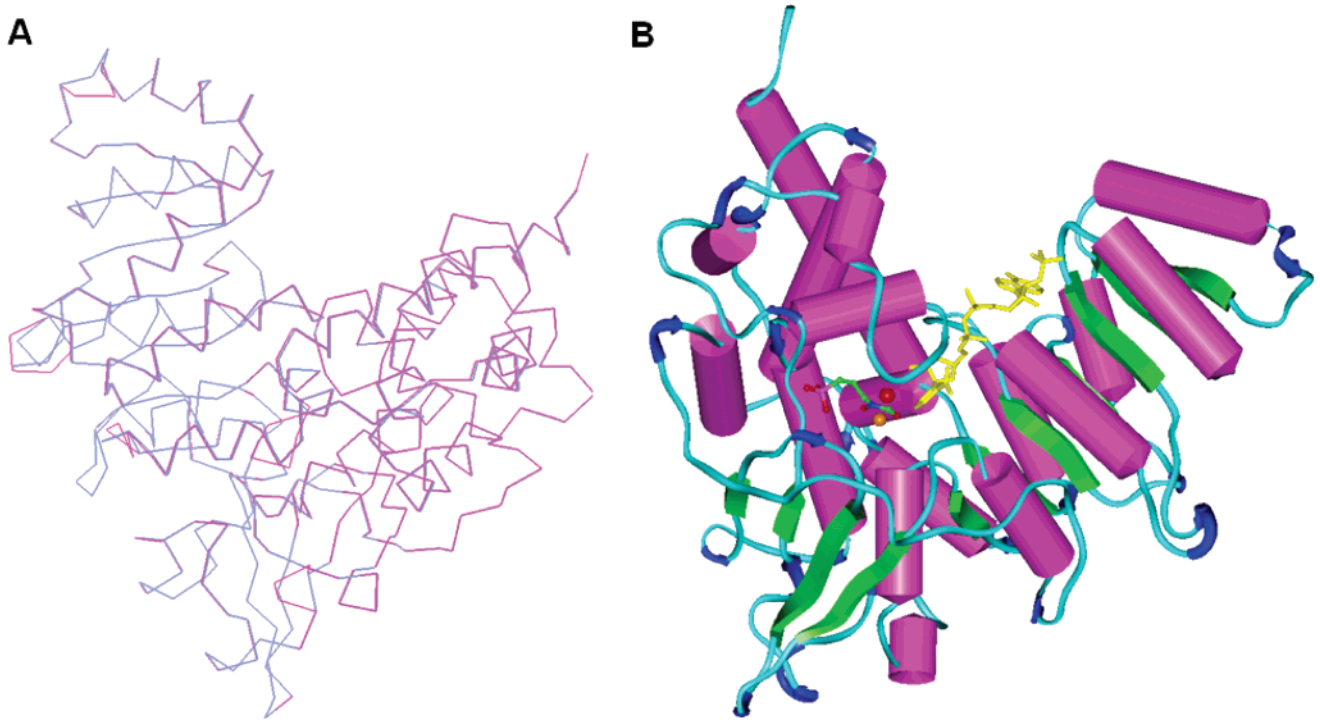

Figure 4. (A) Structure superposition of the modeled structure of *Pf*-DXR (pink) with the X-ray crystal structure of the *Ec*-DXR (blue). Only α-carbons are shown in this picture. (B) Schematic view of the final homology-model of *Pf*-DXR. (NADPH (in yellow) and fosmidomycin (colored by atom type) shown as stick model; Mg^{2+} ion in orange; critical binding site water in red.) Helices and sheets are represented as pink cylinders and green arrows, respectively.

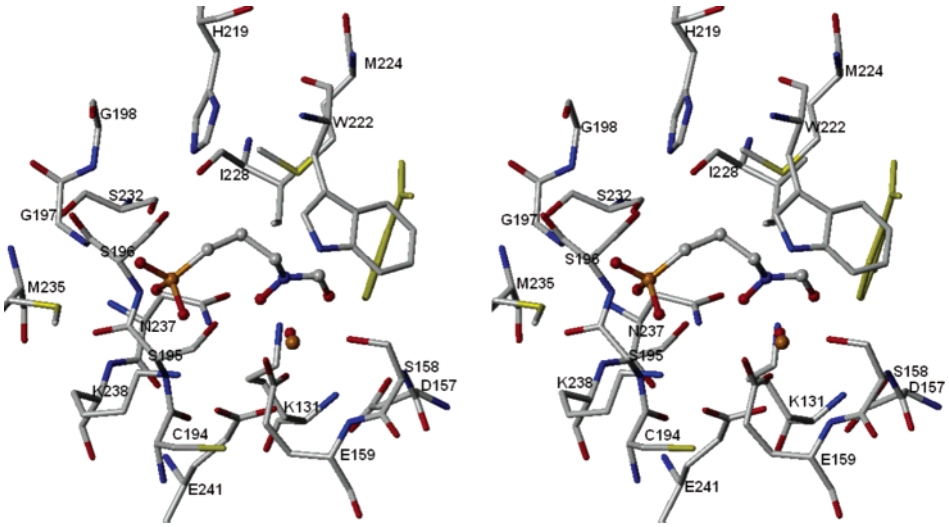

Figure 5. Stereoscopic view of the binding mode of fosmidomycin within the active site of *Pf*-DXR with a prominent hydrophilic cavity: Fosmidomycin represented as a ball-and-stick model; NADPH indicated in yellow; metal ion and water molecule in orange and red, respectively.

orientation as a restraint for the subsequent modeling process. The resulting complex was then refined iteratively by performing stepwise energy minimization and optimization in an aqueous environment.

The refined 3D structure of *Pf*-DXR generated by the homology modeling method is displayed in Figure 4. The backbone RMSD between the final minimized homology model and the template, *E. coli* crystal structure is 1.77 Å, while that between the starting homology-modeled structure and the template was only 1.02 Å; therefore, the minimization did not appear to cause a substantial distortion in the structure and accomplished the goal of relieving steric clashes and close contacts. The small RMSD can also be interpreted to mean that the two structures share common homology and the generated structure is reasonable.

The superimposition between the present structure and the *E. coli* DXR structure shows that the active site architecture is significantly similar between the two protein structures, with same residues interacting with the inhibitor, fosmidomycin (e.g. Glu159 (Glu152 in *Ec*-DXR), Glu241 (Glu231), Lys238 (Lys228), Asn237 (Asn227), Ser196 (Ser186), Ser232 (Ser222)), Figure 5, although interaction with Ser158 (Ser151) reported in the crystal structure was not observed in the current model. Interactions with Gly197 and His219 were found in *Pf*-DXR that has not been observed in any published crystal structures of DXR. Prior findings indicate

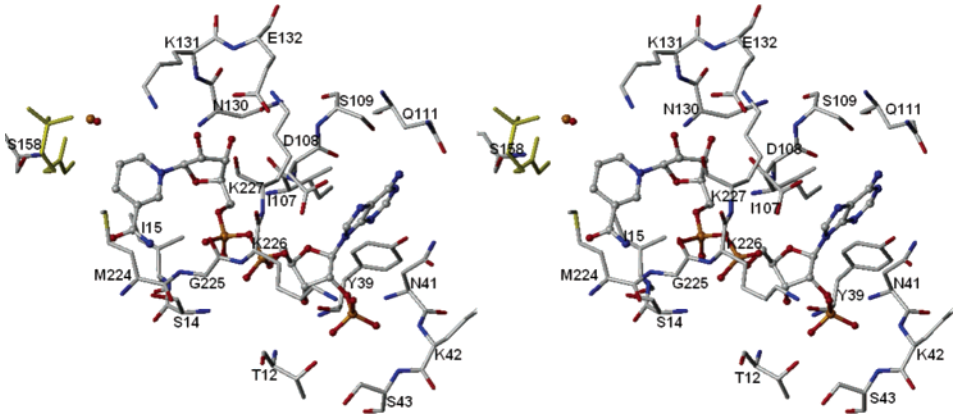

Figure 6. Stereoview of the NADPH binding to *Pf*-DXR: NADPH represented as a ball-and-stick model; fosmidomycin indicated in yellow; metal ion and water molecule in orange and red, respectively.

that His219 (His209 in *Ec*-DXR) is essential for placing the substrate or fosmidomycin in the active site for optimal catalysis.[44] This residue has been implicated to act as a hatch for the flexible loop that closes upon the active site in a tight binding conformation once the substrate or the inhibitor has positioned itself within the binding pocket. In a previous site-directed mutagenesis study, it was demonstrated that mutation of this residue to a glutamine results in significantly decreased affinity toward the substrate, DXP, with an 8-fold increase in the Km (DXP) indicating the importance of this residue.[49] The three hydrophobic methylene groups of the fosmidomycin do not seem to interact with the surrounding residues and, thus, fail to contribute to the high affinity of the inhibitor. The highly conserved residues, Met286, Met224, and Trp222, shield the active site from the solvent molecules. The β-indole of Trp222 is at a distance of 3.91 Å from the carbon backbone of fosmidomycin that provides the key interaction with substrate or fosmidomycin.[43] Overall, the binding site appears to be narrow, and the loop region (Ala211-Gly220) closes tightly upon the active site restricting the access of the larger substrate molecules into the active site.

The folding found in the final model of *Pf*-DXR is very similar to its homologue *Ec*-DXR with the same coordination environment around the catalytic Mg^{2+} ion. The (*N*-formyl-*N*-hydroxy) amino headgroup of fosmidomycin coordinates Mg^{2+} ion forming an octahedral complex with active site residues: Asp157, Glu159, and Glu241 and a critical binding site water molecule. Interestingly, these interactions are in all similar to those established with the *Ec*-DXR enzyme, which is not surprising because *Pf*-DXR shares a high sequence identity at the active site with that of *Ec*-DXR.[43]

During the development of the protein−ligand complex, energy minimization analyses clearly demonstrated a role for both inhibitor and cofactor in the stabilization of the structure of *Pf*-DXR, particularly in relation to the loop region. The cofactor NADPH is bound to *Pf*-DXR in an extended conformation similar to that previously reported for other DXRs[32,48] and extends into the active site. The 2′ phosphate group of NADPH forms a hydrogen bond with Thr12, which is a conserved residue across the DXR family (Figure 6). Hydrogen bond interactions with strictly conserved residues Ile15, Met224, and Met286 further help in anchoring the cofactor into the binding pocket. Nearly the same protein−cofactor interactions are observed (hydrogen bonds seen with residues: Thr12 (Thr10 in *Ec*-DXR), Ser14 (Ser9), Ile15 (Ile10), Lys42 (Lys37), Asp108 (Asp103), and Glu132 (Glu127)). Only one interaction is different, i.e., Gln106 in *Ec*-DXR is not observed in *Pf*-DXR; however, this does not alter the nicotinamide binding property. Additionally, interactions are found with Asn41, Ser43, Gly106, Ile107, Lys226, Asn130, and Lys131. These interactions provide evidence to the fact that NADPH has a vital role in tight binding of the inhibitor within the enzyme active site.

Protein Structure Validation. One essential requisite for a model is to have a good stereochemistry. The refined structure was evaluated for overall quality using available analysis procedures. These analyses compare specific properties of the model with those for known high quality protein structures. For this purpose three protein analysis programs were used: PROCHECK, PROSTAT, and PROFILE-3D.

PROCHECK is a well-known protein structure checking program that provides an assessment of the overall quality of the structure and highlight regions that may need further investigation. The phi-psi plot is shown in Figure 7, while the more detailed results are listed in Table 1. The Ramachandran plot of the model showed a normal distribution of points with phi angles mostly restricted to negative values and psi values clustered in a few distinct regions with the Φ and Ψ angle values for all nonglycyl, nonprolyl residues in the most favored regions (87.6%), additional allowed regions (6.9%), and generously allowed regions (4.7%). Only three residues were found in the disallowed regions. Analysis of the model reveals that these outlying residues are located far from the putative active site of the protein. This good stereochemical quality is not surprising for the high sequence identity (36%) and similarity (60%) between *Ec*-DXR and the target. Figure 7 shows that the structure is reasonable overall because the spot distribution for the homology-modeled structure was similar to the standard X-ray structure. Table 1 lists more detailed scores for both structures. The results showed that our modeled structure was comparable with the standard structures.

Another protein structure analysis program, PROSTAT, was used for structure validation. The program measures all bond distances, bond angles, and dihedral angles for the given protein structure and compare them with its own database. It then lists the number of instances where structural features differ significantly from average values in known proteins.

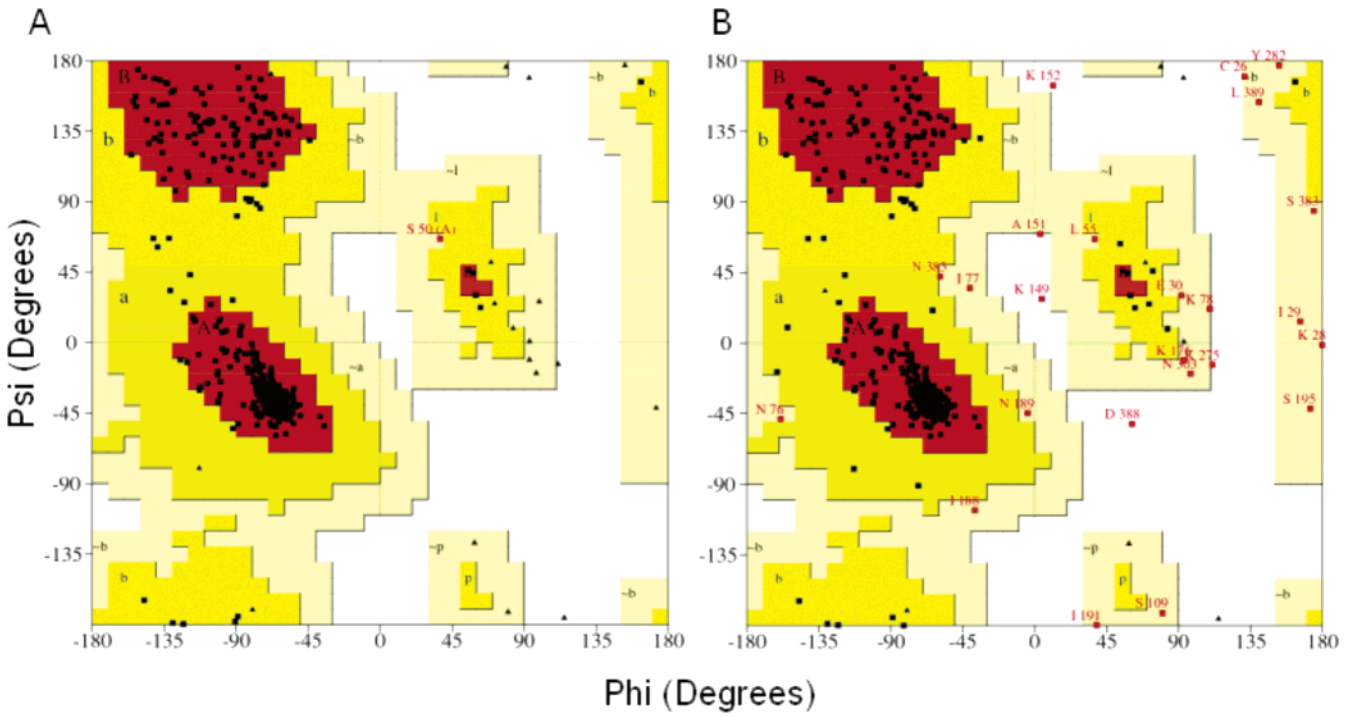

Figure 7. Ramachandran plot of (A) the X-ray structure of *Ec*-DXR (B) and the homology-modeled structure of *Pf*-DXR. The different colored areas indicate "disallowed" (white), "generously allowed" (light yellow), "additional allowed" (yellow), and "most favored" (red) regions (refer to Table 1).

Table 1. Results of Protein Structure Check by PROCHECK and PROSTAT

	Ec-DXR	*Pf*-DXR
residues in most favored regions	332 (93.0%)	338 (87.6%)
residues in additional allowed regions	24 (6.7%)	27 (6.9%)
residues in generously allowed regions	1 (0.3%)	18 (4.7%)
residues in disallowed regions	0 (0%)	3 (0.8%)
number of non-Gly and non-Pro residues	357	386
number of end residues	2	2
number of Gly residues (shown as white boxes)	21	14
number of Pro residues	18	12
total number of residues	398	414
overall PROCHECK score[a]	0.19	−0.48
number of bond distances with significant deviations[b] (by PROSTAT)	0	0
number of bond angles with significant deviations[b] (by PROSTAT)	0	0
number of dihedral angles with significant deviations[b] (by PROSTAT)	2	8

[a] Recommended value > -0.50 and investigation is needed for < -1.0. [b] Number of instances for which the property differs more than 10 standard deviations from the reference value.

The cut-off used for significantly different was 10 standard deviations from the reference value. No spurious angle or bond length was detected in our model. The results are listed at the bottom of Table 1. Using these geometric criteria, the *Pf*-DXR model compares well with the X-ray structure of *Ec*-DXR.

Finally, the 3D homology-modeled structure was verified using the PROFILE-3D program in *InsightII* software (see Supporting Information; Figure S1) and then compared with the template structure. A smoothing window size of 10 residues was used. The analysis yielded a value of 174.78, well within the acceptable range of 84.99−188.87 for a protein of equivalent size, indicating the reliability of the model. For comparison, analysis for the *E. coli* crystal structure was used as the template yielded a score of 181.51, while the range for the structure was 81.68−188.59.

In summary, the above-mentioned analyses indicate that the model structure is consistent with current understanding of protein structure.

Docking Simulations. Docking studies not only provide an understanding of the binding mode of the ligands but also have been employed to validate homology models.[50] Therefore, the task of docking known inhibitors of DXR[43] was undertaken to authenticate the model by calculating the correlation between the pIC_{50} values of the inhibitors and their respective docking scores. Although the published pIC_{50} were obtained with *E. coli* DXR instead of *P. falciparum*, no major differences might be expected since the two proteins share a high sequence identity of 73% at the active site.[43] So far, the only available inhibition data for *P. falciparum* DXR has been published by Jomaa et al. where FR900093 (Figure 2), a fosmidomycin analogue, is shown to be approximately 2−3-fold more active than fosmidomycin both against recombinant *Pf*-DXR and cultured *P. falciparum* parasites. Besides, there is no significant difference with *Ec*-DXR.

Following refinement and validation of the model, fosmidomycin and its analogues were docked into the active

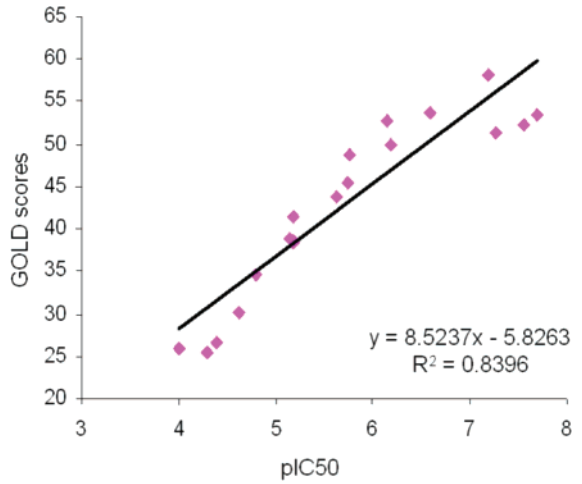

Figure 8. A graph showing the correlation of GOLD scores versus observed activities of fosmidomycin derivatives.

site. Molecular docking can fit molecules together in a favorable configuration to form a complex system. The structural information from the theoretically modeled complex may help us to clarify the catalytic mechanism of enzyme. The genetic algorithm program GOLD was used to perform automated molecular docking. The reliability of the applied docking protocol was assessed by docking fosmidomycin into the active site of modeled *Pf*-DXR. The key characteristic of a good docking program is its ability to reproduce the experimental binding modes of ligands. To test this, a ligand is taken out of the X-ray structure of its protein−ligand complex and docked back into its binding site. The docked binding mode is then compared with the experimental binding mode, and a root-mean-square distance (RMSD) between the two is calculated; a prediction of a binding mode is considered successful if the RMSD is below a certain value (usually 2.0 Å). The RMSD between the docked binding mode and the experimental binding mode for fosmidomycin when docked into the modeled structure was within this cut-off limit (1.42 Å). The cofactor NADPH, Mg^{2+} ion, and a critical water molecule were included in the docking studies to generate more appropriate binding modes by limiting the binding pocket in space. This protocol was then similarly applied to all ligands. For each ligand, 15 solutions were generated. Generated ligand docking solutions mutually differ by RMSD ~1.5 Å.

An analysis of the best docking modes of various docked ligands exhibited common binding characteristics, which may be due to the close structural similarity existing among them. The ability of the hydroxamate group to chelate the Mg^{2+} ion in the active site has been experimentally shown to be important for activity of DXR inhibitors and is supported by docking performed in this study. The hydroxamic acid moiety of all the inhibitors coordinated the metal ion in the active site forming an octahedral complex with three highly conserved active site residues in all DXR family members: Asp157, Glu159, and Glu241 and a water molecule, in a similar fashion as shown for fosmidomycin as well as FR900098 (Figures 6 and 9). Besides, the positioning of phosphonate moiety and its hydrogen-bonding network with amino acid residues is comparable for almost all ligands. Hydrogen bonding interactions are seen with Ser196, Asn237, Lys238, His219, and the phosphonate moiety. The oxygen atom of the carbonyl functionality in all ligands forms hydrogen bonds with Ser158 and Glu159. Also, the oxygen atom in the hydroxyl group makes bifurcated hydrogen bonds with Lys131 and Glu241. In all these interactions are indicative of substrate-like binding of these inhibitors.

The scores calculated for the docked inhibitors are shown in Figure 8 (see Supporting Information, Figure S2). An excellent correlation coefficient of 0.84 between the pIC_{50} values and the GOLD scores was observed. This also highlights the predictive nature of the model to successfully differentiate between the active and the inactive compounds against the enzyme. It is observed that the high scoring ligands (also more active) are generally smaller in size. This indicates that bulky substitutions are not well tolerated perhaps due to steric hindrances by the active site residues. As an example, in Figure 9, the docking of the most potent inhibitor, FR900098, in the modeled *Pf*-DXR structure reveals that the inhibitor places itself in a similar way to fosmidomycin with comparable interactions with the protein active site residues. Although structurally similar to fosmidomycin, its higher activity may be explained on the basis of the additional van der Waals interaction between the

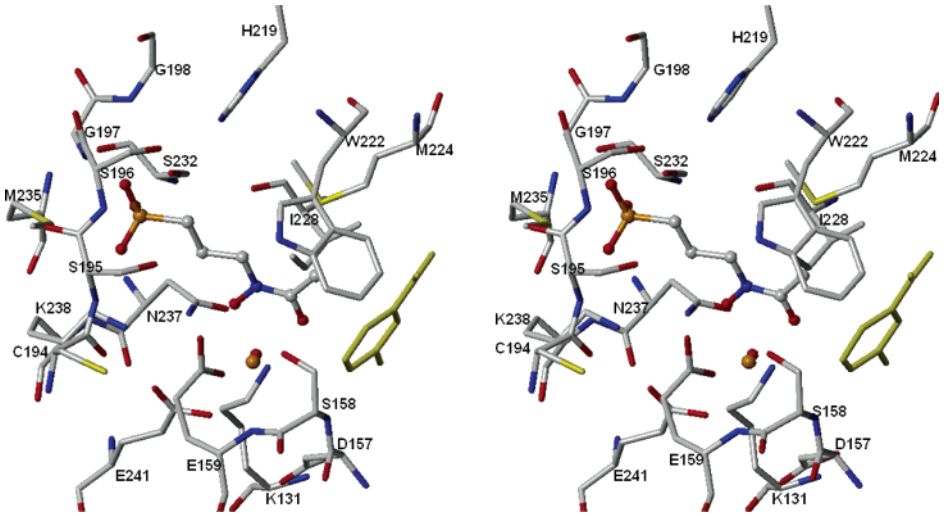

Figure 9. Stereoview of the binding mode of compound 14 (FR900098) docked into the active site of *Pf*-DXR modeled structure. FR900098 represented as a ball-and-stick model; NADPH indicated in yellow; metal ion and water molecule in orange and red, respectively.

methyl group and indole moiety of the active site residue, Trp222.

Thus, the model can explain variations in the pIC_{50} values, which, in turn, is related to binding affinities of the inhibitors, implying that it had been constructed with reasonable accuracy. The results from the docking simulations are self-consistent in that the best docking modes of various inhibitors exhibited common binding characteristics among them, supporting the validity of the model and its suitability for structure based drug design.

CONCLUSIONS

In the present work, a computational approach was utilized to determine the complete three-dimensional structure of *Pf*-DXR, to circumvent the absence of its crystallographic structure. Through several steps of energy minimization and refinement, a model structure of the ligand−enzyme complex was obtained which can be used as a significant tool to enhance our understanding of interaction of DXR inhibitors with the protein at the atomic level. This structure was assessed both by the use of several protein validation tools as well as docking studies. The essential amino acid residues at the active site regions of the generated model are highly conserved. Docking studies were carried out on several known DXR inhibitors using the modeled *Pf*-DXR, and a significant correlation was obtained between ligand binding affinity and empirical docking score. The docking results also indicate that the DXRs have a common ligand docking mode and, perhaps, the same chemical mechanism. Experimental studies are needed to test the structural conclusions and substrate/cofactor requirements deduced from this study. Efforts are underway in our laboratory to identify inhibitors of DXR for their antimalarial and antibacterial potential using this model by in silico docking of large databases of chemical compounds. Overall, the present structure indeed prospects the possibility of using structure-based design to develop inhibitors that are effective against malarial parasites. This approach could facilitate the isolation of completely novel DXP inhibitors and might thus represent an important step toward the establishment of antimalarial chemotherapy.

ACKNOWLEDGMENT

This work was supported by the CDC Cooperative agreement number U01 CI000211. The authors also thank Drs. Babu Lal Tekwani and Prashant Desai for helpful discussions.

Supporting Information Available: Profile 3D plot generated to evaluate the modeled *Pf*-DXR structure (Figure S1) and chemical structures and the corresponding DXR inhibitory activity of the compounds used for automated simulation studies (Figure S2). This material is available free of charge via the Internet at http://pubs.acs.org.

REFERENCES AND NOTES

(1) Carlson, J. C.; Byrd, B. D.; Omlin, F. X. Field assessments in western Kenya link malaria vectors to environmentally disturbed habitats during the dry season. *BMC Public Health* **2004**, *4*, 33−40.

(2) Snow, R. W.; Guerra, C. A.; Noor, A. M.; Myint, H. Y.; Hay, S. I. The global distribution of clinical episodes of *Plasmodium falciparum* malaria. *Nature* **2005**, *434*, 214−217.

(3) Breman, J. G. The ears of hippopotamus: manifestations, determinants, and estimates of the malaria burden. *Am. J. Trop. Med. Hyg.* **2001**, *64*, 1−11.

(4) World Health Organization. WHO expert committee on malaria (twentieth report). *World Health Organ Tech. Rep. Ser.* **2000**, *892*, 1−74 (available online at http://mosquito.who.int/docs/ecr20_toc.htm).

(5) Kreier, J. P. In *Malaria: Epidemiology, Chemotherapy, Morphology, and Metabolism*; New York: Academic Press: 1980; Vol. 1.

(6) Hviid, L. Clinical disease, immunity and protection against *Plasmodium falciparum* malaria in populations living in endemic areas. *Expert Rev. Mol. Med.* **1998**, *1998*, 1−10.

(7) Gardner, M. J.; et al. Genome sequence of the human malaria parasite *Plasmodium falciparum. Nature* **2002**, *419*, 498−511.

(8) (a) Rohmer, M.; Knani, M.; Simonin, P.; Sutter, B.; Sahm, H. Isoprenoid biosynthesis in bacteria: a novel pathway for the early steps leading to isopentenyl diphosphate. *Biochem. J.* **1993**, *295*, 517−524. (b) Broers, S. T. J. Ph.D. Dissertation, Eidgenö ssischen Technische Hochschule Zurich, 1994. (c) Schwarz, M. K. Ph.D. Dissertation, Eidgenö ssischen Technischen Hochschule, Zurich, 1994.

(9) Jomaa, H.; Wiesner, J.; Sanderbrand, S.; Altincicek, B.; Weidemeyer, C.; Hintz, M.; Turbachova, I.; Eberl, M.; Zeidler, J.; Lichtenthaler, H. K.; Soldati, D.; Beck, E, Inhibitors of the nonmevalonate pathway of isoprenoid biosynthesis as antimalarial drugs. *Science* **1999**, *285*, 1573−1575.

(10) Takahashi, S.; Kuzuyama, T.; Watanabe, H.; Seto, H. A. 1-deoxy-D-xylulose 5-phosphate reductoisomerase catalyzing the formation of 2-C-methyl-D-erythritol 4-phosphate in an alternative nonmevalonate pathway for terpenoid biosynthesis. *Proc. Natl. Acad. Sci. U.S.A.* **1998**, *95*, 9879−84.

(11) Proteau, P. J. 1-Deoxy-D-xylulose 5-phosphate reductoisomerase: an overview. *Bioorg. Chem.* **2004**, *32*, 483−493.

(12) Lange, B. M.; Croteau, R. Isopentenyl diphosphate biosynthesis via a mevalonate-independent pathway: isopentenyl monophosphate kinase catalyzes the terminal enzymatic step. *Proc. Natl. Acad. Sci. U.S.A.* **1999**, *96*, 13714−13719.

(13) Bochar, D. A.; Friesen, J. A.; Stauffacher, C. V.; Rodwell, V. W. In *Comprehensive Natural Product Chemistry*; Pergamon: Oxford, 1999; p 1544.

(14) Sprenger, G. A.; Schorken, U.; Wiegert, T.; Grolle, S.; de Graaf, A. A.; Taylor, S. V.; Begley, T. P.; Bringer-Meyer, S.; Sahm, H. Identification of a thiamin-dependent synthase in *Escherichia coli* required for the formation of the 1-deoxy-D-xylulose 5-phosphate precursor to isoprenoids, thiamin, and pyridoxol. *Proc. Natl. Acad. Sci. U.S.A.* **1997**, *94*, 12857−12862.

(15) Schwender, J.; Seemann, M.; Lichtenthaler, H. K.; Rohmer, M. Biosynthesis of isoprenoids (carotenoids, sterols, prenyl side-chains of chlorophylls and plastoquinone) via a novel pyruvate/glyceraldehyde 3-phosphate non-mevalonate pathway in the green alga Scenedesmus obliquus. *Biochem. J.* **1996**, *316*, 73−80.

(16) Mueller, C.; Schwender, J.; Zeidler, J.; Lichtenthaler, H. K. Properties and inhibition of the first two enzymes of the non-mevalonate pathway of isoprenoid biosynthesis. *Biochem. Soc. Trans.* **2000**, *28*, 792−793.

(17) Qureshi, A. A.; Porter, J. W. In *Biosynthesis of Isoprenoids*; Spurgeon, S. L., Ed.; John Wiley: New York, 1981; pp 47−94.

(18) Lois, L. M.; Campos, N.; Putra, S. R.; Danielsen, K.; Rohmer, M.; Boronat, A. Cloning and characterization of a gene from *Escherichia coli* encoding a transketolase-like enzyme that catalyzes the synthesis of D-1-deoxyxylulose 5-phosphate, a common precursor for isoprenoid, thiamin, and pyridoxol biosynthesis. *Proc. Natl. Acad. Sci. U.S.A.* **1998**, *95*, 2105−2110.

(19) Lell, B.; Ruangweerayut, R.; Wiesner, J.; Missinou, M. A.; Schindler, A.; Baranek, T.; Hintz, M.; Hutchinson, D.; Jomaa, H.; Kremsner, P. G. Fosmidomycin, a novel chemotherapeutic agent for malaria. *Antimicrob. Agents Chemother.* **2003**, *47*, 735−738.

(20) Kuzuyama, T.; Shimizu, T.; Takahashi, S.; Seto, H. Fosmidomycin, a specific inhibitor of 1-deoxy-D-xylulose 5-phosphate reductoisomerase in the nonmevalonate pathway for terpenoid biosynthesis. *Tetrahedron Lett.* **1998**, *39*, 7913−7916.

(21) Rohdich, F.; Wungsintaweekul, J.; Fellermeier, M.; Sagner, S.; Herz, S.; Kis, K.; Eisenreich, W.; Bacher, A.; Zenk, M. H. Cytidine 5′-triphosphate-dependent biosynthesis of isoprenoids: YgbP protein of *Escherichia coli* catalyzes the formation of 4-diphosphocytidyl-2-C-methylerythritol. *Proc. Natl. Acad. Sci. U.S.A.* **1999**, *12*, 96, 11758−63.

(22) Fiser, A.; Sanchez, R.; Melo, F.; Sali, A. Comparative protein structure modeling. In *Computational Biochemistry and Biophysics*; Watanabe, B., Roux, A., MacKerell, A. D., Jr.; Becker, O. M., Eds.; Marcel Dekker: New York, 2001; pp 275−312.

(23) Lesk, A. M.; Chothia, C. How different amino acid sequences determine similar protein structures: the structure and evolutionary dynamics of the globins. *J. Mol. Biol.* **1980**, *136*, 225−270.

(24) Chothia, C.; Lesk, A. M. The relation between the divergence of sequence and structure in proteins. *EMBO J.* **1986**, *5*, 823−826.

(25) Burley, S. K. An overview of structural genomics. *Nat. Struct. Biol.* **2000**, (suppl.) *7*, 932−934.

(26) Kroemer, R. T.; Doughty, S. W.; Robinson, A. J. Prediction of the three-dimensional structure of human interleukin-7 by homology modeling. *Protein Eng.* **1996**, *9*, 493−498.
(27) Baker, D.; Sali, A. Protein structure prediction and structural genomics. *Science* **2001**, *294*, 93−96.
(28) Boeckmann, B.; Bairoch, A.; Apweiler, R.; Blatter, M. C.; Estreicher, A.; Gasteiger, E.; Martin, M. J.; Michoud, K.; O'Donovan, C.; Phan, I.; Pilbout, S.; Schneide, M. The SWISS−PROT protein knowledge base and its supplement TrEMBL in 2003. *Nucl. Acids Res.* **2003**, *31*, 365−370.
(29) Thompson, J. D.; Higgins, D. G.; Gibson, T. J. CLUSTAL W: Improving the sensitivity of progressive multiple sequence alignment through sequence weighting, position-specific gap penalties and weight matrix choice. *Nucl. Acids Res.* **1994**, *22*, 4673−80.
(30) Rost, B.; Sander, C.; Prediction of protein secondary structure at better than 70% accuracy. *J. Mol. Biol.* **1993**, *232*, 584−599.
(31) InsightII Accelrys Inc., 9685 Scranton Road, San Diego, CA 92121-3752, U.S.A.
(32) Mac Sweeney, A.; Lange, R.; Fernandes, R. P.; Schulz, H.; Dale, G. E.; et al. The crystal structure of *E. coli* 1-deoxy-D-xylulose-5-phosphate reductoisomerase in a ternary complex with the antimalarial compound fosmidomycin and NADPH reveals a tight-binding closed enzyme conformation. *J. Mol. Biol.* **2005**, *345*, 115−127.
(33) Adrian, A.; Canutescu, A.; Shelenkov, A.; Dunbrack, R. L., Jr. A graph-theory algorithm for rapid protein side-chain prediction. *Protein Sci.* **2003**, *12*, 2001−2014.
(34) (a) Dunbrack, R. L., Jr.; Karplus, M. Conformational analysis of the backbone-dependent rotamer preferences of sidechains. *Nat. Struct. Biol.* **1994**, *1*, 334−340. (b) Bower, M. J.; Cohen, F. E.; Dunbrack, R. L., Jr. Prediction of protein side-chain rotamers from a backbone-dependent rotamer library: a new homology modeling tool. *J. Mol. Biol.* **1997**, *267*, 1268−1282.
(35) Flohil, J. A.; Vriend, G.; Berendsen, H. J. C. Completion and refinement of 3-D homology models with restricted molecular dynamics: Application to targets 47, 58, and 111 in the CASP modeling competition and posterior analysis. *Proteins: Struct., Funct., Genet.* **2002**, *48*, 593−604.
(36) Yin, X.; Proteau, P. J. Characterization of native and histidine-tagged deoxyxylulose 5-phosphate reductoisomerase from the cyanobacterium Synechocystis sp. PCC6803. *Biochim. Biophys. Acta* **2003**, *1652*, 75−81.
(37) Argyrou, A.; Blanchard, J. S. Kinetic and chemical mechanism of *Mycobacterium tuberculosis* 1-deoxy-D-xylulose-5-phosphate isomeroreductase. *Biochemistry* **2004**, *43*, 4375−4384.
(38) Koppisch, A. T.; Fox, D. T.; Blagg, B. S. J.; Poulter, C. D. *E. coli* MEP synthase: steady-state kinetic analysis and substrate binding. *Biochemistry* **2002**, *41*, 236−243.
(39) Bock, C. W.; Katz, A. K.; Markham, G. D.; Glusker, J. P. Manganese as a replacement for magnesium and zinc: functional comparison of the divalent ions. *J. Am. Chem. Soc.* **1999**, *121*, 7360−7372.
(40) Laskowski, R. A.; MacArthur, M. W.; Moss, D. S.; Thornton, J. M. PROCHECK: a program to check the stereochemical quality of protein structures. *J. Appl. Crystallogr.* **1993**, *26*, 283−291.
(41) Jones, G.; Willett, P.; Glen, R. C.; Leach, A. R.; Taylor, R. Development and validation of a genetic algorithm for flexible docking. *J. Mol. Biol.* **1997**, *267*, 727−748.
(42) Verdonk, M. L.; Cole, J. C.; Hartshorn, M. J.; Murray, C. W.; Taylor, R. D. Improved protein−ligand docking using GOLD *Proteins: Struct., Funct., Genet.* **2003**, *52*, 609−623.
(43) Silber, K.; Heidler, P.; Kurz, T.; Klebe, G. AFMoC enhances predictivity of 3D QSAR: A case study with DOXP-reductoisomerase. *J. Med. Chem.* **2005**, *48*, 3547−3563.
(44) Yajima, S.; Nonaka, T.; Kuzuyama, T.; Seto, H.; Ohsawa, K. Crystal structure of 1-deoxy-D-xylulose 5-phosphate reductoisomerase complexed with cofactors: implications of a flexible loop movement upon substrate binding. *J. Biochem. (Tokyo)* **2002**, *131*, 313−317.
(45) Steinbacher, S.; Kaiser, J.; Eisenreich, W.; Huber, R.; Bacher, A.; et al. Structural basis of fosmidomycin action revealed by the complex with 2-C-methyl-D-erythritol 4-phosphate synthase (IspC). Implications for the catalytic mechanism and antimalaria drug development. *J. Biol. Chem.* **2003**, *278*, 18401−18407.
(46) Berman, H. M.; Westbrook, J.; Feng, Z.; Gilliland, G.; Bhat, T. N.; et al. The Protein Data Bank. *Nucleic Acids Res.* **2000**, *28*, 235−242.
(47) Yajima, S.; Hara, K.; Sanders, J. M.; Yin, F. L.; Ohsawa, K.; et al. Crystallographic structures of two bisphosphonate: 1-deoxyxylulose-5-phosphate reductoisomerase complexes. *J. Am. Chem. Soc.* **2004**, *126*, 10824−10825.
(48) Ricagno, S.; Grolle, S.; Bringer-Meyer, S.; Sahm, H.; Lindqvist, Y.; et al. Crystal structure of 1-deoxy-d-xylulose-5-phosphate reductoisomerase from *Zymomonas mobilis* at 1.9-Å resolution. *Biochim. Biophys. Acta* **2004**, *1698*, 37−44.
(49) Kuzuyama, T.; Takahashi, S.; Takagi, M.; Seto, H. Characterization of 1-Deoxy-D-xylulose 5-Phosphate Reductoisomerase, an enzyme involved in isopentenyl diphosphate biosynthesis, and identification of its catalytic amino acid residues. *J. Biol. Chem.* **2000**, *275*, 19928−19932.
(50) Folkers, G. Integrated homology modeling and X-ray study of herpes simplex virus I thymidine kinase. In *Structure-based drug design experimental and computational approaches*; Codding, P. W., Ed.; Kluwer Academic Publishers: Norwell, MA, U.S.A., 1998; pp 271−283.

CI050523W